Macromolecular Bioscience
www.mbs-journal.de

3D Porous Binary Composites of Collagen, Elastin, and Fibrin Proteins Orchestrate Adipose Tissue Regeneration

Prasad Sawadkar, Nandin Mandakhbayar, Kapil D Patel, Nazanin Owji, Poojitha Rajasekar, Roudin Sarama, Jung-Hwan Lee, Hae-Won Kim, Jonathan Knowles, and Elena García-Gareta*

The objective for this study is to advance the development of a specialized biomaterial that can effectively facilitate the regeneration of adipose tissue. In prior studies, the assessment of collagen (Col), elastin (Ela), and fibrin (Fib) unary scaffolds has been conducted. However, it is important to note that native adipose tissue is comprised of a diverse array of extracellular matrix (ECM) constituents. To mimic this behavior, binary compositions of collagen, elastin, and fibrin are fabricated in a 1:1 ratio, resulting in the formation of Col/Ela, Col/Fib, and Ela/Fib composites through a customized fabrication procedure. The physical properties of these scaffolds are comprehensively analyzed using a range of material characterization techniques. Additionally, the biological properties of the scaffolds are investigated by examining the survival, proliferation, and phenotype of adipose-derived stem cells. Subsequently, the aforementioned binary scaffolds are implanted into a rodent model for 28 days. the explants are analysed through X-ray microtomography, histology, and immunohistochemistry. The findings of the study demonstrate that the utilization of binary combinations of Col/Ela, Col/Fib, and Ela/Fib has a discernible impact on the physical and biological characteristics of the scaffolds. Nevertheless, Ela/Fib exhibits characteristics that make it a suitable candidate for adipogenesis due to its notable upregulation of caveolin-1 expression in both acellular and cellular cohorts. The combination of two natural polymers in this cell–material interaction has significantly enhanced the comprehension of adipogenesis.

1. Introduction

Repairing soft-tissue defects post curative surgery and traumatic rupture is a clinical challenge. Current surgical treatments include grafting and implant-based strategies, but both these methods hold substantial drawbacks. For example, autograft recipients are at risk of wound infection and flap failure, whereas implant-based strategies involve risk of extrusion, leakage/rupture, adverse immune reaction, and rejection.[1]

In the last few decades, there is a quest to design an ideal biomaterial to attempt to harness the regenerative capacity of the body to overcome challenges encountered by traditional procedures. These biomaterials are fabricated with natural and/or synthetic polymers, and both these polymeric approaches have their own advantages over others. In this study, we aim to design an ideal biomaterial for adipogenesis with naturally occurring proteins present in the human body, such as collagen (Col), elastin (Ela), and fibrin (Fib). Collagen is an abundant natural protein in extracellular matrix (ECM) and is widely used as a biomaterial because of its wide applicability and less

P. Sawadkar, R. Sarama
The Griffin Institute
Northwick Park Institute for Medical Research
Northwick Park and St Mark's Hospitals
London, HA1 3UJ, UK
E-mail: prasad.sawadkar@ucl.ac.uk

The ORCID identification number(s) for the author(s) of this article can be found under https://doi.org/10.1002/mabi.202400073

© 2024 The Author(s). Macromolecular Bioscience published by Wiley-VCH GmbH. This is an open access article under the terms of the Creative Commons Attribution License, which permits use, distribution and reproduction in any medium, provided the original work is properly cited.

DOI: 10.1002/mabi.202400073

P. Sawadkar, N. Owji, E. García-Gareta
Regenerative Biomaterials Group
The RAFT Institute at The Griffin Institute
Northwick Park & Saint Mark's Hospitals
London, HA1 3UJ, UK

P. Sawadkar
Division of Surgery and Interventional Science
University College London
London, WC1E 6BT, UK

P. Sawadkar, K. D Patel, J.-H. Lee, H.-W. Kim, J. Knowles
UCL Eastman-Korea Dental Medicine Innovation Centre
Dankook University
Cheonan 31114, Republic of Korea

P. Sawadkar
Department of Metabolism
Digestion and Reproduction
Faculty of Medicine
Imperial College London
London, SW7 2AZ, UK

immunogenicity.[2–4] Fibrin is a natural matrix formed by the polymerization of fibrinogen and thrombin that provides biomechanical cues for cell migration and activates various signaling cascades for tissue repair.[5,6] Elastin is an ECM protein that provides elasticity to the body, and it is present in connective tissues. In humans, elastin is coded by the ELN gene and is hierarchically assembled from tropoelastin, a precursor of elastin bundles to form elastic fibers. The expression of the ELN gene is at its peak in early development and decreases in the later stage of life.[7–9] Elastin has a half-life of 74 years; hence, it is an ideal candidate for our natural polymer selection.[10]

Stem-cell-based therapies are becoming popular in clinic due to their plasticity and self-renewing ability, and they fall under embryonic stem cell (ESC), induced pluripotent stem cell (iPSC), and mesenchymal stem cell (MSC) groups. In this study, we have studied cells and binary scaffold interaction using human adipose-derived stem cells (hADSCs). A primary reason for this is that ADSCs are multipotent and present in the native fat tissue; hence, anatomically, they are easily accessible clusters of putative stem cells for therapeutic use. Current methods for harvesting ADSCs are ultrasound-assisted, power-assisted, and laser-assisted liposuction and excision of fat tissue.[11,12]

Previously we demonstrated how unary natural proteins such as collagen, elastin, and fibrin orchestrate adipogenesis by their physical, in vitro and in vivo biological properties.[13] However, native adipose tissue is not made up of unary protein but is a combination of several proteins. Therefore, to understand this mechanism, this study aimed to investigate how binary combinations of collagen, elastin, and fibrin (1:1) and in conjunction with adipose-derived stem cells can affect adipogenesis in a 3D environment in vivo in the rodent model.

N. Mandakhbayar, K. D Patel, J.-H. Lee, H.-W. Kim, J. Knowles
Institute of Tissue Regeneration Engineering (ITREN)
Dankook University
Cheonan 330-714, Republic of Korea

N. Mandakhbayar, K. D Patel, J.-H. Lee, H.-W. Kim, J. Knowles
Department of Nanobiomedical Science & BK21 Plus NBM Global Research Centre for Regenerative Medicine
Dankook University
Cheonan 330-714, Republic of Korea

N. Mandakhbayar, J.-H. Lee, H.-W. Kim, J. Knowles
Department of Biomaterials Science
School of Dentistry
Dankook University
Cheonan 31116, Republic of Korea

K. D Patel, N. Owji, J. Knowles, E. García-Gareta
Division of Biomaterials and Tissue Engineering
UCL Eastman Dental Institute
University College London
London, WC1E 6BT, UK

P. Rajasekar
Division of Respiratory Medicine
University of Nottingham
Nottingham, NG7 2UH, UK

E. García-Gareta
Multiscale in Mechanical & Biological Engineering Research Group
Aragón Institute of Engineering Research (I3A)
School of Engineering & Architecture
University of Zaragoza
Zaragoza, Aragón 50018, Spain

2. Experimental Section

2.1. Scaffold Fabrication

2.1.1. Collagen Solution

In 90% type I rat tail collagen (First Link, Birmingham, UK) was added to 10% (v/v) of 10× minimal essential medium (Invitrogen, Paisley, UK). This solution was neutralized using 5 and 1 M sodium hydroxide.

2.1.2. Elastin Solution

10% (v/v) bovine elastin powder (Sigma, UK) was mixed with 0.5 M oxalic acid (freshly prepared) at room temperature.

2.1.3. Fibrin Solution

2% bovine fibrinogen (Sigma, UK) was dissolved in 1× phosphate-buffered saline (PBS) and 10% bovine thrombin. To fabricate three different binary composite scaffolds, collagen/elastin (Col/Ela) (1:1 v/v; collagen/fibrin (Col/Fib), (1:1 v/v); and elastin/fibrin (Ela/Fib), (1:1 v/v) were used (**Figure 1**). All composites were chemically crosslinked using 3% glutaraldehyde as a homo-bifunctional cross-linker agent and lyophilized to form a disk-shaped scaffold of ≈ 13 mm (diameter) × 4 mm (thickness) in dimension.

2.2. Swelling Ratio

The following equation was used to calculate the scaffold's swelling ratio

$$\mathrm{SR} = \frac{M_w - M_d}{M_w} \times 100 \quad (1)$$

where M_d is the dry mass (measured at time 0) and M_w is the wet mass of the scaffold,[13] which was calculated by immersing the scaffold into 5 mL of distilled water for 15 min at 37 °C.

2.3. Dynamic Water Contact Angle

In this study, the wettability of the scaffolds surfaces by intermolecular interaction was determined by calculating the dynamic water contact angle (dWCA). For this purpose, 30 µL of distilled water droplet was dispensed onto each scaffold and its absorption pattern was video recorded. At each time point, screenshots were taken and the dWCA calculated using the principle of Young's equation with ImageJ (1.8.0_112) software. (NIH, USA).

2.4. Surface Architecture

Scaffolds were washed in deionized water to remove excess salts and mounted on stubs followed by sputter-coating with a carbon coater. All images were obtained using a secondary electron detector in a Philips XL 30 Field Emission SEM, operated at 5 kV with an average working distance of 10 mm.

© 2024 The Author(s). Macromolecular Bioscience published by Wiley-VCH GmbH

16165195, 0, Downloaded from https://onlinelibrary.wiley.com/doi/10.1002/mabi.202400073 by Universidad De Zaragoza, Wiley Online Library on [19/06/2024]. See the Terms and Conditions (https://onlinelibrary.wiley.com/terms-and-conditions) on Wiley Online Library for rules of use; OA articles are governed by the applicable Creative Commons License

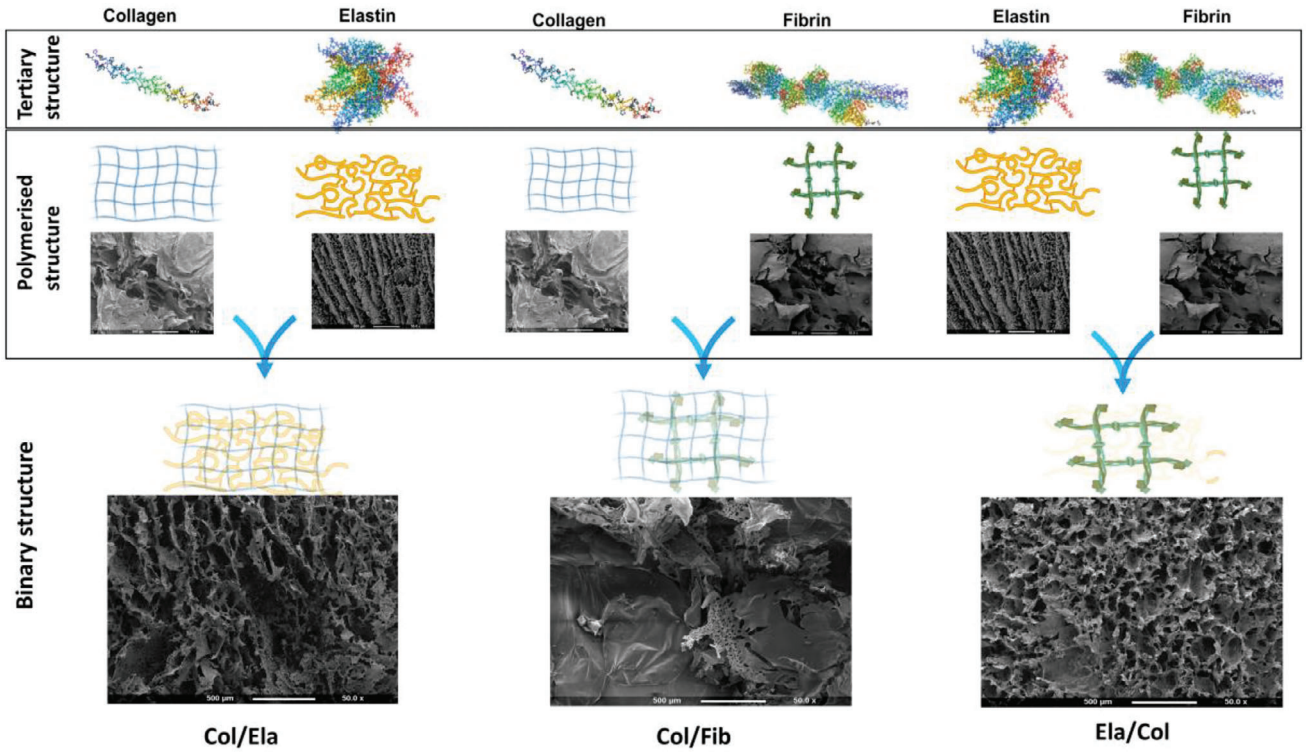

Figure 1. Schematic representation of binary fabrication of Col/Ela, Col/Fib, and Ela/Fib scaffolds with SEM structure of scaffolds at 50×.

2.5. Biaxial Mechanical Testing

The mechanical test for 3D scaffolds was performed using biaxial mechanical set-up. The set-up for the mechanical test was designed similar to the in vivo biomechanical environment. Prior to the mechanical test, 3D scaffolds were submerged in PBS bath at 37 °C for 15 min, and the specimen dimensions (length and diameter) were measured. Next, an equi-biaxial tensile test was conducted using BioTester (CellScale Biomaterials Testing, Canada) in displacement control with load cells of 23 N. The test was performed for pre-condition of five cycles at 0.25 Hz.

2.6. Fourier-Transform Infrared Spectroscopy and Thermal Gravimetric Analysis

The scaffolds (before and after crosslinking) were characterized by attenuated total reflectance Fourier transformed infrared spectroscopy (ATR-FTIR, Varian 640-IR, Australia) and thermal gravimetric analysis (TGA, N-1500; Scinco, South Korea). The TGA of scaffolds was carried out using a portion of the samples in the presence of nitrogen gas flow at temperature from 25 to 800 °C, with a heating rate of 10 °C min^{-1}.

2.7. In Vitro hADSC Seeding

Human adipose-derived stem cells (ATCC, UK) were cultured in MesenPRO RS basal cell culture medium (ThermoFisher, UK) supplemented with 2% MesenPRO RS growth supplement (ThermoFisher, UK) and 1% penicillin/streptomycin (Sigma–Aldrich, UK) at 37 °C with 5% CO_2. Scaffolds were seeded with 7.5×10^5 cells at passages 3 or 4.

2.8. Cell Viability and Proliferation

Cell viability of hADSC was assessed by a double staining kit (Sigma–Aldrich, UK) where an assay solution of 10 µL of calcein-AM and 5 µL propidium iodide (PI) was prepared in 5 mL of in PBS and added to the scaffold and incubated at 37 °C with 5% CO_2 for 30 min. Live and dead cells were visualized by fluorescence imaging and confocal microscopy (Leica DM IRE2 confocal microscope). The quantitative rate of cell proliferation on scaffolds was measured using a resazurin-based AlamarBlue (BIO-RAD, UK) assay. An assay solution of 1:10 (v/v) AlamarBlue was prepared in culture media, added to the cells, and incubated at 37 °C with 5% CO_2 for 3 h. Following the manufacturer's instructions, absorbance was measured at 570 with 600 nm as reference wavelength by using a double beam UV–visible spectrophotometer (Spectronic Camspec Ltd., Garforth, UK).

2.9. hADSC Differentiation Study

RNA was isolated from the cells at days 3, 7, and 14 using a TRIzol-based (Invitrogen, Paisley, UK) method. The yield was quantified by spectrophotometry (Spectronic Camspec Ltd., Garforth, UK) followed by complementary DNA (cDNA) synthesis using Precision nanoscript 2 reverse transcription kit (Primer

© 2024 The Author(s). Macromolecular Bioscience published by Wiley-VCH GmbH

16165195, 0, Downloaded from https://onlinelibrary.wiley.com/doi/10.1002/mabi.202400073 by Universidad De Zaragoza, Wiley Online Library on [19/06/2024]. See the Terms and Conditions (https://onlinelibrary.wiley.com/terms-and-conditions) on Wiley Online Library for rules of use; OA articles are governed by the applicable Creative Commons License

Table 1. Forward and reverse primer.

Name of gene	Forward primer	Reverse primer	Accession number
MYOD1	CGCCTGAGCAAAGTAAATGAG	GCCCTCGATATAGCGGATG	NM_002478
PPARG	GAATAAAGATGGGGTTCTCATATCC	AACTTCAGCAAACTCAAACTT	NM_138711
CEBPA	CGGCAACTCTAGTATTTAGGATAAC	CAAATAAAATGACAAGGCACGATT	NM_004364
RUNX2	TTCTCCCCTTTTCCCACTGA	CAAACGCAATCACTATCTATACCAT	NM_004348
SOX9	GGACCAGTACCCGCACTTG	AATCCGGGTGGTCCTTCTTG	NM_000346
OCT4	CACTAAGGAAGGAATTGGGAACA	GGGATTAAAATCAAGAGCATCATTG	NM_002701
REX1	CGTTTCGTGTCCCTTTCA	CCTCTTGTTCATTCTTGTTCGTATT	NM_174900

Design, Southampton, UK). A quantitative polymerase chain reaction (q-PCR) was performed with custom designed and synthesized primers (**Table 1**) (Primer design, Southampton, UK).

2.10. Isolation, Identification, and Culture of Rat Adipose-Derived Stem Cells

In order to seed scaffolds with rat adipose-derived stem cells (rADSC) for the in vivo experiments, three female rats were euthanized and white adipose tissue (WAT) was isolated from inguinal, anterior, and retroperitoneal fat pads. WAT was minced thoroughly with a sterile scalpel and digested with pre-warmed 0.2% collagenase I and 0.075% collagenase II in PBS for 2 h at 37 °C. Collagenases were then inactivated by adding fetal bovine serum (FBS) and centrifuged at 800 × *g* for 10 min at room temperature. A cell pallet was re-suspended in RBC lysis buffer (1:9, v/v) and incubated for 10 min at room temperature, immediately centrifuged at 800 × *g* for 10 min and re-suspended in 20 mL of proliferation medium. The cell suspension was filtered through a 100 µm nylon mesh cell strainer and cultured at 37 °C and 5% CO_2 for 24 h, after which nonadherent cells were removed. Finally, cells were passaged twice after reaching 70% confluence level (18).

To identify pure rADSC population, staining of cell surface markers was performed followed by flow cytometry using BD FACSARIA III (BD Biosciences, NJ, USA). Cell population tested positive for CD 105, CD 90, CD 73, and negative for CD 31, CD 34 (Figure S1, Supporting Information). Furthermore, cultured rADSC's differentiation potential was tested for adipogenic, osteogenic, and chondrogenic lineages using Oil Red O, alkaline phosphatase (ALP) staining, and Alcian blue staining, respectively (Figure S2, Supporting Information). In the cellular group, scaffolds were seeded with rADSC (1×10^6 cells per scaffold) and incubated at 37 °C with 5% CO_2 for 4 h to allow cell attachment.

2.11. In Vivo Implantation

The animal husbandry and experimental protocols used in this study were approved by the Animal Care and Use Committee at Dankook University, Republic of Korea. For this work, six Sprague–Dawley, 9–10 weeks old (170–210 g), healthy male rats were used, and the study was divided into two groups, namely acellular (scaffold) and cellular group (scaffold + rADSC). All surgeries were performed under general anesthesia, which was induced by intramuscular injection of a mixture of ketamine (80 mg kg^{-1}) and xylazine (10 mg kg^{-1}). The dorsal region was shaved and disinfected with iodine solution before making an incision of 2 cm in the dorsal medial region. Four scaffolds per animal were implanted in each side of the anterior and posterior regions within intercostal space. At day 28, rats were anesthetized under isoflurane, and 420 mg kg^{-1} Ioversol (Optiray 350 Rx, Guerbet LLC, USA), an iodine-based compound, was injected into the left ventricle to visualize blood vessels into the scaffold. After 15 min, rats were euthanized by CO_2 inhalation and scaffolds with the surrounding tissue were harvested and fixed in 10% neutral buffered formalin (NBF) for 2 h at room temperature for further analysis.

2.12. X-Ray Micro-Computed Tomography

Pre- and post-implanted scaffolds were wrapped in a transparent plastic film and mounted for scanning using submicron resolution micro-CT (Skyscan 1176, Skyscan, Belgium). For each section, a scan was performed at 45 kV X-ray voltage with a 0.2 mm aluminum filter, a source current of 556 µA, 0.5° rotation step, and an exposure time of 180 ms. 3D models were reconstructed using Skyscan NRecon software (Bruker micro-CT, Belgium). In order to analyze pore size, pore thickness, porosity percentage (%) by CTAn software (Bruker micro-CT, Belgium), angiogenesis by CTVol software (Bruker micro-CT, Belgium) and volume degradation by CTVox (Bruker micro-CT, Belgium), reconstructed datasets were processed after segmentation and binarization.

2.13. Histological Analysis

Samples fixed in 10% NBF were processed for paraffin histology and cut into 3 µm thick sections that were stained for haematoxylin and eosin (H&E). Additionally, collagen-based scaffolds were stained with Sirius Red, fibrin scaffolds with Martius Scarlet and Blue (MSB), and elastin scaffolds with Elastin Van Gieson stain (EVG).

2.14. Statistical Analysis

All experiments were carried out with minimum three repeats ($n = 3$). Results were presented as mean ± standard deviation.

© 2024 The Author(s). Macromolecular Bioscience published by Wiley-VCH GmbH

16165195, 0, Downloaded from https://onlinelibrary.wiley.com/doi/10.1002/mabi.202400073 by Universidad De Zaragoza, Wiley Online Library on [19/06/2024]. See the Terms and Conditions (https://onlinelibrary.wiley.com/terms-and-conditions) on Wiley Online Library for rules of use; OA articles are governed by the applicable Creative Commons License

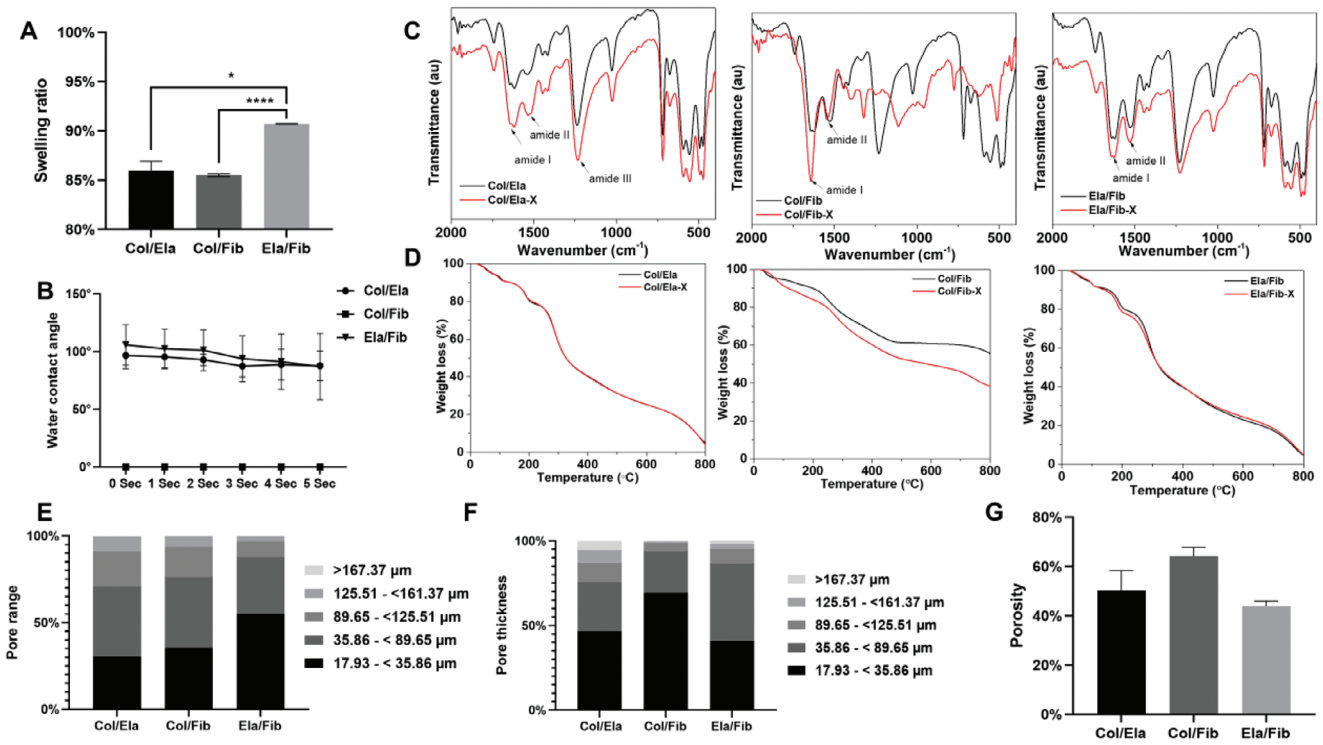

Figure 2. A) Swelling ratio of the scaffolds (* $p < 0.05$ and **** $p < 0.0001$). B) Water contact angle (WCA). C) Fourier-transform infrared spectroscopy (FTIR) for Col/Ela, Col/Fib, and Ela/Fib. D) Thermal gravimetric analysis (TGA) for Col/Ela, Col/Fib, and Ela/Fib, where X indicates crosslinked scaffolds. Pore properties of scaffolds measured using µCT: E) pore range, F) pore thickness, and G) porosity.

Statistical analysis was carried out by two-way analysis of variance (ANOVA) at 95% confidence interval with two tail alpha levels of 0.05, (*p*-value) using GraphPad Prism 7.03 (GraphPad Software, Inc, CA, USA).

3. Results and Discussion

3.1. Physical Properties of Scaffolds

The swelling ratio of any material is a competition in which the solvent is trying to attain equilibrium through penetrating inside the polymeric scaffolds. Due to a sudden influx of solvent, the polymeric network inside these scaffolds begins to elongate by generating an elastic retractive force to oppose this deformation.[3] Therefore, swelling ratios were a simple method to understand the polymeric network in our scaffolds. Col/Ela (85.93 ± 0.97%) and Col/Fib (85.51 ± 0.13%) showed similar swelling ratios, but for Ela/Fib (90.70 ± 0.04%) this ratio was significantly higher (**Figure** 2A). These results were interesting and related to our previous findings with the unary combination of elastin where the swelling ratio was 35.73 ± 77%.[13] However, combining elastin with collagen and fibrin resulted in a higher swelling ratio. We had shown that our elastin scaffolds were hydrophobic as elastin is an insoluble protein, whereas collagen and fibrin scaffolds were hydrophilic. This trend continued in the binary combinations as the calculated WCA for Col/Fib was 0.00. Even though collagen and fibrin scaffold were hydrophilic in unary form but the binary combination with elastin resulted in a more hydrophobic nature as calculated WCA for Col/Ela was 96.63 ± 11.49, Ela/Fib was 105.80 ± 17.60. This showed the physical properties of elastin superseded collagen and fibrin's properties in binary combination (Figure 2B).

3.2. Chemical Structure and Properties of Scaffolds

The ATR-FTIR spectra of the scaffold prepared by binary compositions of the proteins with and without crosslinking are shown in Figure 2C. The FTIR spectra of collagen–elastin and elastin–fibrin binary compositions with crosslinked (Col/Ela-X) and without crosslinked Col/Ela) do not show any change. The peaks at 1617–1642, 1516–1535, and 1230 cm^{-1} are the characteristic peaks of collagen and elastin, and associated with amide I, amide II, and amide III, respectively.[13] However, the FTIR spectra of collagen–fibrin binary composition with crosslinking (Col/Fib-X) and without crosslinking (Col/Fib) exhibit significant change. Post crosslinking collagen-fibrin scaffold showed a sharp and intense peak at 1643 cm^{-1} associated with amide I and predominantly corresponds to the C═O stretching, amide II peak shifted from 1529.25 to 1545.86 cm^{-1}, and amide III peak at 1228.59 cm^{-1} is reduced to a small and weak peak after crosslinking. Moreover, peaks at 1738.75, 1024.57, 718.75, 674.47, 594.78, 556.05, 492.59, and 473.41 cm^{-1} disappeared and new peaks at 1400.87, 1322.66, 113.12, 958.54, 773.72, 625.01, 514.73, and 426.56 cm^{-1} appeared. The disappearance of peaks and appearance of new ones in Col/Fib-X scaffold confirmed the chemical interaction between collagen and fibrin during glutaraldehyde crosslinking and changed the secondary structure of the proteins.

© 2024 The Author(s). Macromolecular Bioscience published by Wiley-VCH GmbH

16165195, 0, Downloaded from https://onlinelibrary.wiley.com/doi/10.1002/mabi.202400073 by Universidad De Zaragoza, Wiley Online Library on [19/06/2024]. See the Terms and Conditions (https://onlinelibrary.wiley.com/terms-and-conditions) on Wiley Online Library for rules of use; OA articles are governed by the applicable Creative Commons License

The TGA of binary compositions of collagen, elastin, and fibrin protein scaffolds before and after crosslinking with glutaraldehyde are shown in Figure 2D. The result of temperature-dependent weight loss of Col/Ela and Ela/Fib before (and after crosslinking (Col/Ela-X and Ela/Fib-X) reveals no change. The thermal degradation of collagen–elastin and elastin–fibrin binary scaffolds exhibits similar behaviors and underwent weight loss in three stages: the first stage shows an initial 10.69 ± 1.25% weight loss between 20 and 150 °C, which represents the evaporation of physisorbed water molecules; second stage weight loss of 54.42 ± 1.12% between 150 and 450 °C, which represents thermal degradation of fibrous structures of collagen, fibrin, and elastin; and third stage weight loss of 30.67 ± 0.61% between 450 and 800 °C, which corresponds to the carbonization of residual organic components. The thermal degradation behavior of collagen–fibrin binary scaffolds (Col/Fib and Col/Fib-X) showed a significant difference. In both scaffolds, that is Col/Fib, Col/Fib-X involved the three-stage thermal degradation with initial 15.42 and 19.95% weight losses in the first stage between 20 and 250 °C, respectively, representing the evaporation of physiosorbed water molecules. In the second stage, Col/Fib and Col/Fib-X showed 22.99% and 24.38%, respectively, between 250 and 500 °C, which represent thermal degradation of fibrous structures of collagen and elastin, carbonization of residual organic components such as C═O, N─C═O, primary and secondary amides and major denaturation behavior reported for native elastin.[5,6] The third stage showed significantly different weight loss between Col/Fib and Col/Fib-X, without crosslinked (Col/Fib) exhibited 5.92% and with crosslinked (Col/Fib-X) 14.43% weight loss between 500 and 800 °C, which corresponds to native degradation of carbons and other functional groups such as amides and carboxyl. The significant difference in weight loss in the third stage can be interpreted as the effect of crosslinking and change in the secondary structure of the proteins.

3.3. Architectural Properties of Scaffolds

Our scaffolds were fabricated by lyophilization; hence, we could not control its architecture, but cell spatial distribution and proliferation are determined by the scaffold; hence, understanding the scaffold's pore properties was a crucial parameter. In the literature, the majority of studies determined pore properties using 2D SEM images of dry images, but in vivo cell attachment and proliferation occur in the hydrated state of scaffolds; hence, we evaluated pore properties in a pseudophysiological hydrated environment using micro-CT. In our scaffolds, pore range distribution of Col/Ela and Col/Fib showed a marginal similarity from 17.93 to >167.37 µm scaffold, and Ela/Fib had 55.10% pores from 17.93 to <35.86 µm range, and 32.49% from 35.86 to <89.65 µm range (Figure 2E). In our previous finding, we found that collagen had 41.33%, 86% of elastin, and 32% of fibrin pores distributed in the range from 17.93 to <35.86 µm whereas 34% of collagen, 44% of fibrin, and 90% of elastin pores were in the 35.86–89.65 µm range.[13] However, in the binary combination, Col/Ela's 30.45% and Ela/Fib's 55.10% of pores were in the range from 17.93 to <35.86 µm and 40% in the range from 35.86 to <89.65 µm. This alteration in the pore range distribution was due to the crossover of these proteins during the fabrication process. However, a similar trend was seen for pore thickness; as per our previous finding, collagen and fibrin's 50% and elastin's 86% pore thicknesses were in the range from 17.93 to <35.86 µm but in the binary combination of Col/Fib 69.37% of them and 46.42% for Col/Ela were between 17.93 and <35.86 µm and Ela/Fib the majority of pore thickness (45.58%) range was from 35.86 to <89.65 µm (Figure 2F). This modification in the pore size and thickness has varied porosity of binary scaffolds as Col/Fib was the most porous scaffold with 64.19% of porosity and Col/Ela had 50.22% of porosity in this group, and the least porous scaffold was Ela/Fib with 44% (Figure 2G). This heterogeneity in the pore's properties altered extracellular microenvironments; hence, we have observed variations in water contact angle, swelling ratio, and degradation.

We were also able to study the impact of pore properties on mechanical properties, which are critically important for cell attachment and migration: Col/Ela (*X*-axis = 74.78 ± 19.9 mN and *Y*-axis = 18.32 ± 6.89 mN), Col/Fib (*X*-axis = 154.67 ± 19.21 mN and *Y*-axis = 136.54 ± 18.4 mN), and Ela/Fib (*X*-axis = 116.21 ± 12.98 mN and *Y*-axis = 83.56 ± 7.21 mN) (**Figure 3A–C**). However, the majority of scaffold's mechanical properties are studied by uniaxial testing (longitudinal *X*-axis), but in physiological conditions, the force exerted on the implanted scaffold is 3D; hence, uniaxial force measurements are not ideal.[14] To address this issue, we mechanically tested our scaffold in a pseudo-physiological environment. These studies on pore and mechanical properties have given insight to fabricate a tailored scaffold for adipogenesis.

3.4. In Vitro Biological Properties of Scaffolds

All three scaffolds showed a steady increase in viability and proliferation of the hADSCs. We have previously demonstrated that collagen-based scaffolds showed the highest proliferation and aggregated cellular morphology, but elastin showed distinct spindle morphology with nonaggregated behavior, and fibrin showed weaker cell attachment.[13] In the binary combination of scaffolds, an identical phenomenon was observed, such as the behavior of hADSCs on collagen-based scaffolds (Col/Ela and Col/Fib) outdistanced elastin- and fibrin-based scaffolds due to the ligand-binding receptor for integrin (**Figure 4**).[15] In Ela/Fib scaffolds at day1, cells showed aggregated morphology because of fibrin, but this morphology was superseded by distant nonaggregated morphology because of elastin, as we previously demonstrated.[13,16] Therefore, we can conclude that the cellular architecture and behavior of hADSCs on these scaffolds were influenced by material and chemical properties.

3.5. Gene Expression

Gene expression of five lineage-specific differentiation markers—Myogenic Differentiation 1 (MYOD1); adipogenic differentiation markers: CAAT/enhancer-binding proteins alpha (CEBPα) and peroxisome proliferator-activated receptor-gamma (PPARγ); osteogenic marker: RUNX family transcription factor 2 (RUNX2); chondrogenic marker: SRY-box transcription factor 9 (SOX9); and two pluripotency markers: reduced expression protein 1 (REX1) and octamer-binding protein 4 (OCT4)—was investigated in hADSCs cultured in the three biomimetic binary

© 2024 The Author(s). Macromolecular Bioscience published by Wiley-VCH GmbH

16165195, 0, Downloaded from https://onlinelibrary.wiley.com/doi/10.1002/mabi.202400073 by Universidad De Zaragoza, Wiley Online Library on [19/06/2024]. See the Terms and Conditions (https://onlinelibrary.wiley.com/terms-and-conditions) on Wiley Online Library for rules of use; OA articles are governed by the applicable Creative Commons License

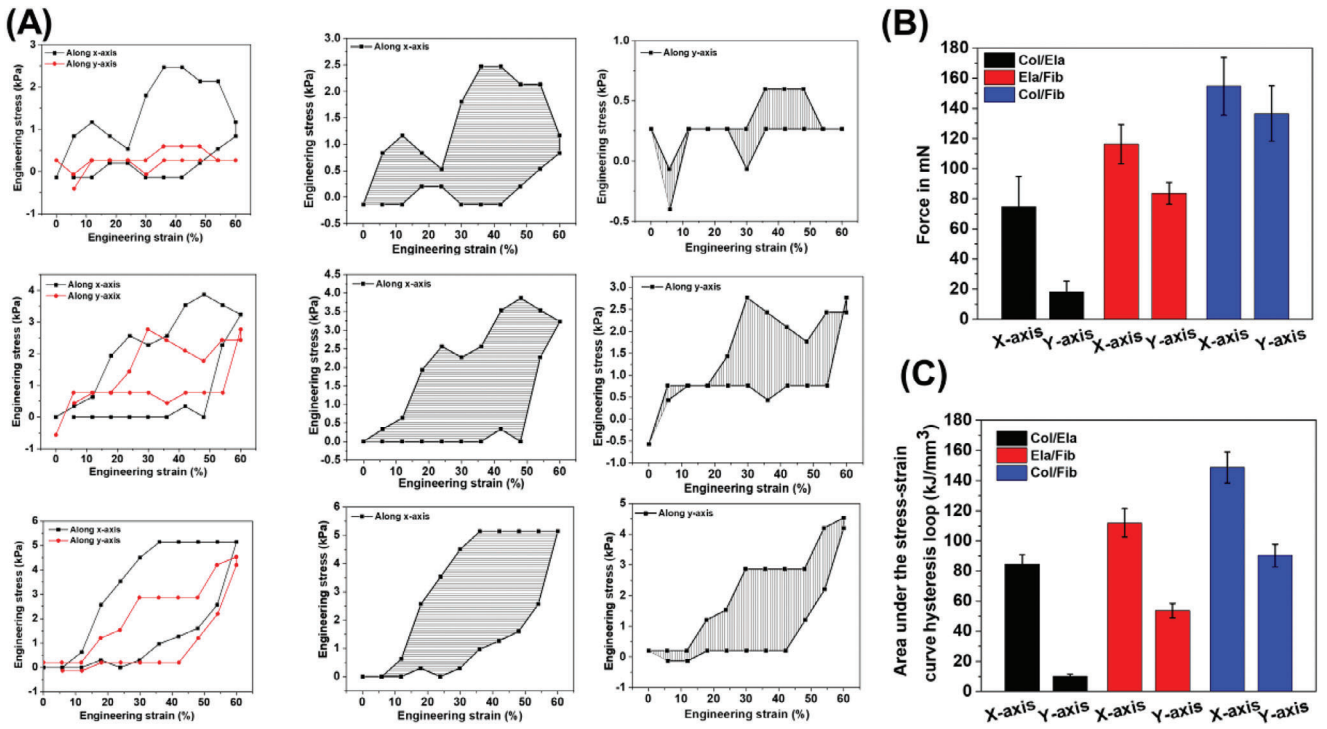

Figure 3. Mechanical properties of the scaffolds in a pseudo-physiological environment using biaxial mechanical testing (longitudinal (*X*) and transverse (*Y*)-axes, A) stress and strain curve, B) maximum force in mN, and C) area under stress–strain hysteresis loop.

scaffolds.[17] Expression of these genes was evaluated at 7, 14, and 21 days to investigate the ability of these scaffolds to induce hADSC differentiation in the absence of external stimuli. hADSCs cultured on tissue culture plastic were used as control. Gene expression has been reported as absolute copy numbers of messenger RNA (mRNA) computed from the standard curve as described in our recent report and housekeeping genes (Figure S3, Supporting Information).[14] We have previously assessed the differentiation of hADSC cultured in collagen, elastin, and fibrin scaffolds individually at days 3, 7, and 14. Expression of pluripotency markers OCT4 and REX1 exhibited significant downregulation across all three time points compared to control suggesting a reduction in stemness of the hADSCs cultured in these biomimetic scaffolds even at 3 days. Collagen scaffold displayed considerable upregulation of all lineage markers, specifically adipogenic marker CEBPα, while elastin and fibrin scaffolds did not show substantial upregulation of lineage-specific differentiation markers.[14] In line with this finding, it was intriguing to understand the differential properties of binary combinations of these biomimetic natural polymers. In this study, we observed significant reduction of OCT4 copy number ($p < 0.01$) at all three time points across the three scaffolds. Col/Fib displayed maximum reduction in copy number from 386 584 copies μL^{-1} in control to less than 250 copies at all time points. REX1 expression was observed to be low (<100 copies μL^{-1}) in control and continued reducing significantly ($p < 0.05$) to less than 20 copies μL^{-1} at all time points in Col/Fib (**Figure 5B**). Low basal level of REX1 in hADSCs has been previously reported in comparison to peripheral blood derived stem cells.[18] Col/Ela and Ela/Fib exhibited an increasing trend in REX1 expression at day 21, although not significantly (Figure 5A,C). CE scaffold exhibited a similar expression profile to collagen scaffold reported in our previous work.[14] In Col/Ela, there was a significant increase in expressions of CEBPα, MYOD1, RUNX2, and SOX9 on day 21. Late-stage adipogenic marker, CEBPα, that exhibited negligible expression in control and day 7 (<10 copies μL^{-1}) was observed to increase by 236-folds at 21 days compared to control. Peroxisome proliferator-activated receptor gamma (-PPARG), on the other hand, remained at negligible levels in Col/Ela through all time points (<60 copies μL^{-1}) similar to the observation in individual collagen and elastin scaffolds in our previous study.[19] hADSC cultured in collagen scaffold displayed a 263-fold increase in CEBPα copy number at day 14, while Col/Fib scaffold takes up to 21 days to match this level of increase. This suggests that collagen retains its pro-adipogenic function even in combination with elastin, which seldom induced adipogenesis in ADSC when used on its own.[19] Following CEBPα, the second highest increase in copy number for hADSC cultured in Col/Ela at day 21 was observed in chondrogenic differentiation marker SOX9. It increased from 76 copies μL^{-1} in control to 1500 copies μL^{-1} at day 21 ($p < 0.001$). Osteogenic marker RUNX2 showed a significant increase in copy number at day 21 ($p < 0.001$), although the measure was very low (111 copies μL^{-1}). Collagen scaffold on its own was observed to induce a 112-fold increase in RUNX2 copy number at day 14 in hADSC.[14] Similar to the trend observed in CEBPα, RUNX2 expression is also attenuated in COl/Ela scaffold compared to collagen only scaffold. Myogenic marker MYOD1 displayed a gradual increase in copy number through the time points and registered a twofold increase at day 21

© 2024 The Author(s). Macromolecular Bioscience published by Wiley-VCH GmbH

16165195, 0, Downloaded from https://onlinelibrary.wiley.com/doi/10.1002/mabi.202400073 by Universidad De Zaragoza, Wiley Online Library on [19/06/2024]. See the Terms and Conditions (https://onlinelibrary.wiley.com/terms-and-conditions) on Wiley Online Library for rules of use; OA articles are governed by the applicable Creative Commons License

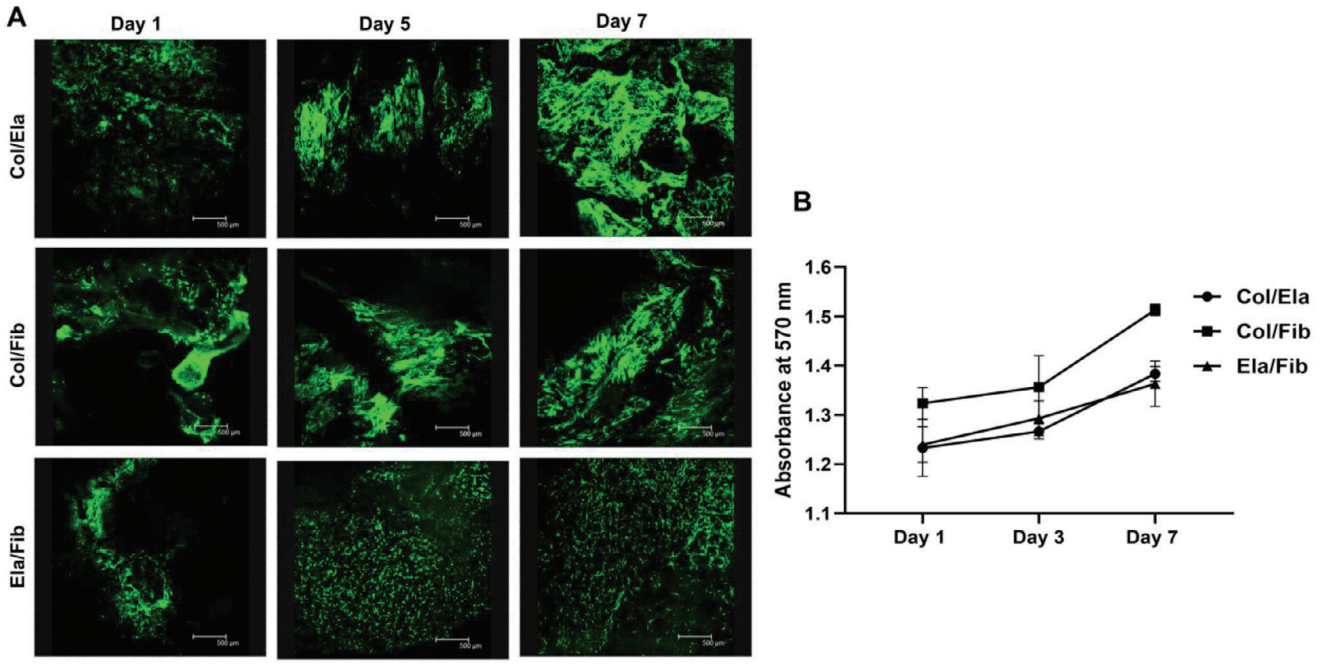

Figure 4. A) Live/dead assay and cellular behavior on the scaffold for days 1, 3, and 7. B) Alamar blue absorbance at 570 nm for days 1, 3, and 7.

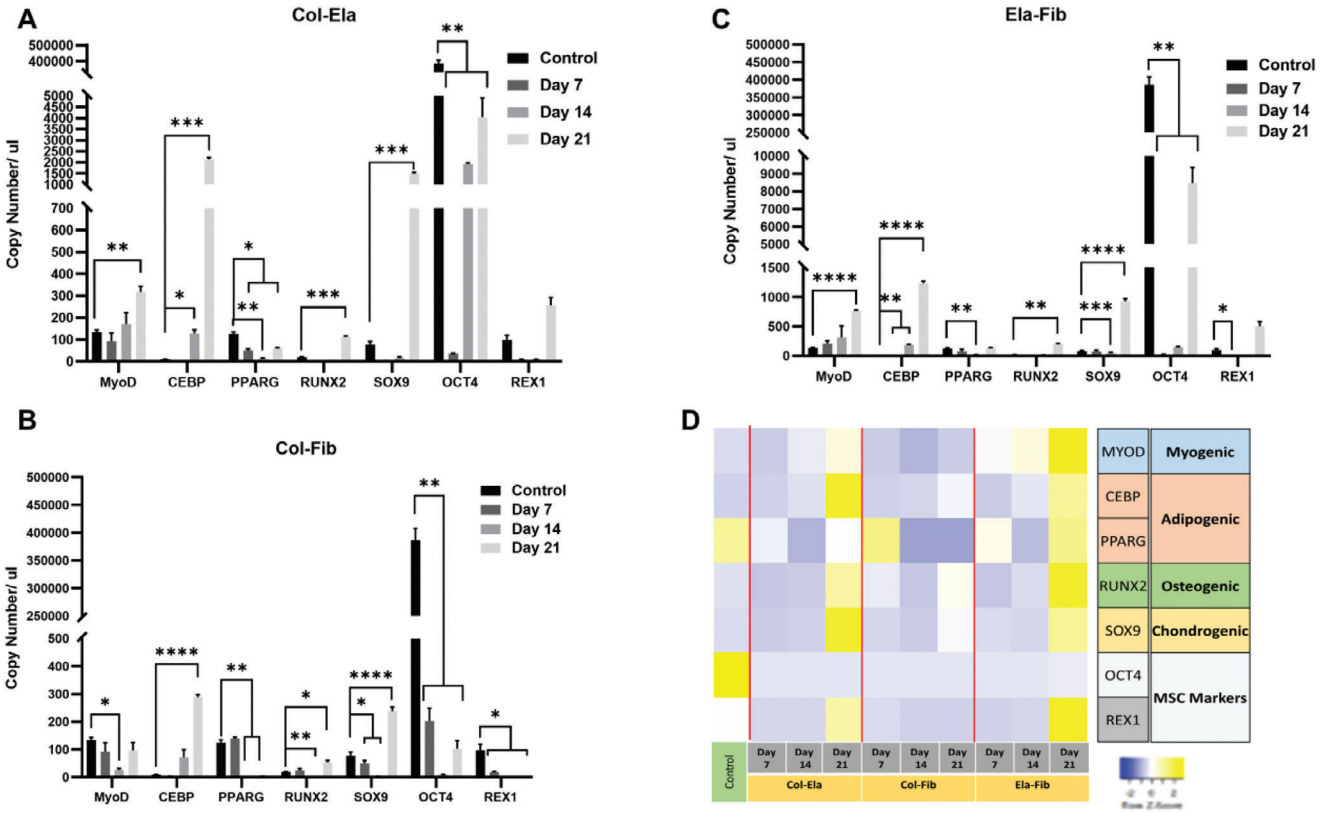

Figure 5. q-PCR results for A) Col/Ela, B) Col/Fib, and C) Ela/Fib (* $p < 0.05$, ** $p < 0.01$, ** $p < 0.001$, and **** $p < 0.0001$). D) Heat map of gene expression.

© 2024 The Author(s). Macromolecular Bioscience published by Wiley-VCH GmbH

16165195, 0, Downloaded from https://onlinelibrary.wiley.com/doi/10.1002/mabi.202400073 by Universidad De Zaragoza, Wiley Online Library on [19/06/2024]. See the Terms and Conditions (https://onlinelibrary.wiley.com/terms-and-conditions) on Wiley Online Library for rules of use; OA articles are governed by the applicable Creative Commons License

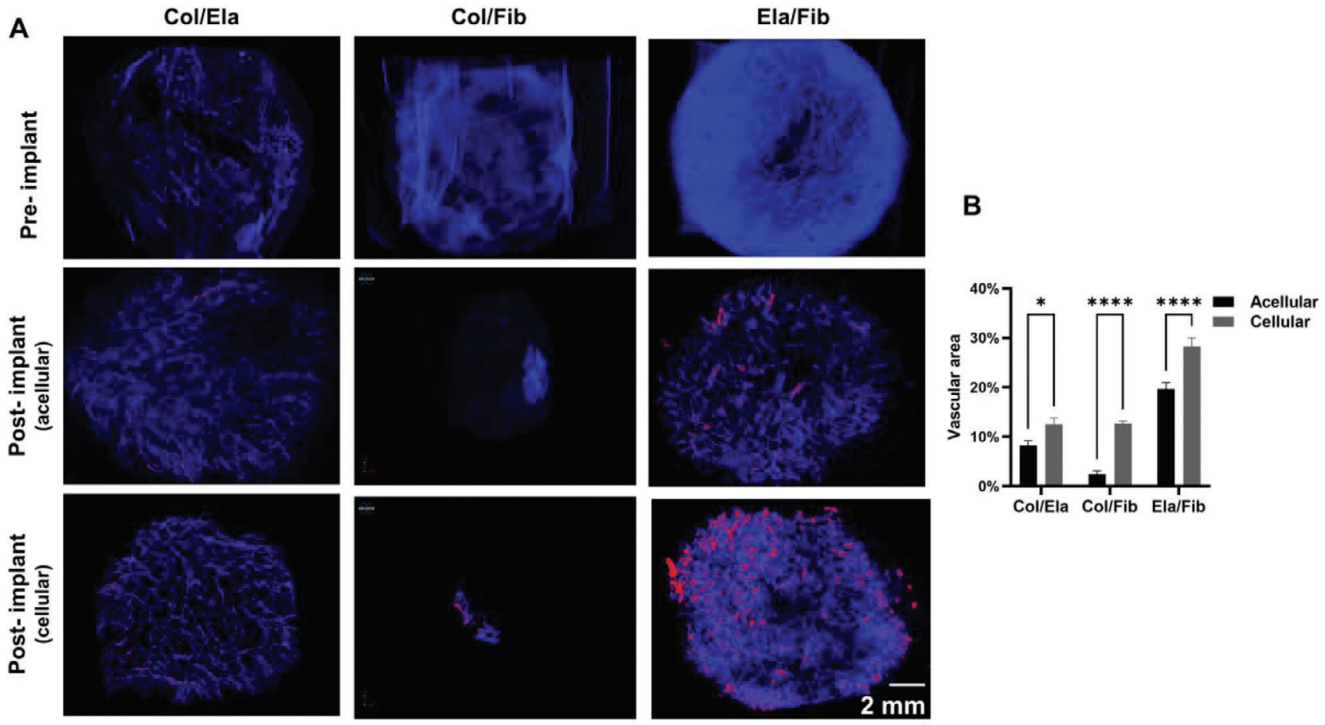

Figure 6. A) Pre-implanted 3D structure of the scaffold under μCT and angiogenesis (red color) in vivo acellular and cellular scaffolds after 28 days, and B) quantification of angiogenesis (* $p < 0.05$, **** $p < 0.0001$).

compared to control in hADSC cultured on CE (Figure 5A). This trend is identical to what was previously observed in hADSC cultured in elastin scaffold. However, hADSC grown in elastin scaffold produced a sixfold increase in copy number at day 14 compared to mere twofold increase at day 21 observed in Col/Ela.[13] It is to be noted that MYOD1 was the only differentiation marker that significantly increased in expression when hADSCs were cultured on an elastin scaffold.[13] These results from hADSC cultured in Col/Ela, combined with the evidence from our previous work in collagen and elastin scaffolds, on their own suggest that combining collagen and elastin retain the differential properties of both natural polymers but lean more toward adipogenic and chondrogenic lineages. Although elastin selectively induced a myogenic shift in hADSC, this effect is not profound in combination with collagen. It is to be noted that hADSC cultured in fibrin scaffold did not show any remarkable increase in lineage-specific differentiation markers.[13] However, fibrin in combination with elastin was observed to show a significant 136-fold increase in CEBPα ($p < 0.0001$) and 5-fold increase in MYOD1 ($p < 0.0001$). In addition, osteogenic and chondrogenic markers RUNX2 and SOX9 also exhibited significant 10-fold and 12-fold increases in copy number at day 21 (Figure 5C). This is a feature that was seen in neither of the components in Ela/Fib scaffold when hADSCs were cultured in them independently. Collagen with its strong differentiation potential was observed to induce differentiation of hADSC in combination with fibrin. hADSC cultured in Col/Fib scaffold displayed a small but significant increase in chondrogenic marker SOX9 (threefolds; $p < 0.0001$) copy numbers at day 21. There was a 32-fold increase in CEBPα (289 copies μL^{-1}) at day 21 compared to control (9 copies μL^{-1}) in hADSC cultured in CF (Figure 5B). This suggests that collagen retains its differential characteristics in Col/Fib by shifting hADSC slightly toward adipogenic and chondrogenic lineages, but the effect may be attenuated due to the addition of fibrin. Out of the three natural biomimetic polymers investigated, collagen seems to have strongest differential ability specifically toward adipogenic and chondrogenic lineages. This feature is retained when collagen is combined with either elastin or fibrin, with elastin proving to be more effective than fibrin in terms of hADSC shift toward adipogenic differentiation.

3.6. Angiogenesis

The gross observation showed that all scaffolds were viable and were able to integrate into host tissue (**Figure 6**A). A cascade of de novo blood vessels is an essential process for any implanted biomaterial to survive as diffusion of oxygen is limited in tissue, and angiogenesis is a fundamental process of tissue regeneration. Additionally, native adipose tissue is a significantly vascularized tissue in the body; hence, to fabricate functional scaffolds for adipose tissue engineering it was a prerequisite to investigate the angiogenetic properties of our scaffolds.[20,21] To visualize blood vessels in our scaffolds, we injected a contrast agent prior to light up the vascular network and post μCT scanning, and we quantified the vascular area. Previously we demonstrated that in the presence of $\alpha 1\beta 1$, $\alpha 2\beta 1$, and $\alpha 11\beta 1$ integrin receptor, collagen-based scaffolds enhanced endothelial docking and resulted in higher vascularization of the scaffold in the binary combination

© 2024 The Author(s). Macromolecular Bioscience published by Wiley-VCH GmbH

16165195, 0, Downloaded from https://onlinelibrary.wiley.com/doi/10.1002/mabi.202400073 by Universidad De Zaragoza, Wiley Online Library on [19/06/2024]. See the Terms and Conditions (https://onlinelibrary.wiley.com/terms-and-conditions) on Wiley Online Library for rules of use; OA articles are governed by the applicable Creative Commons License

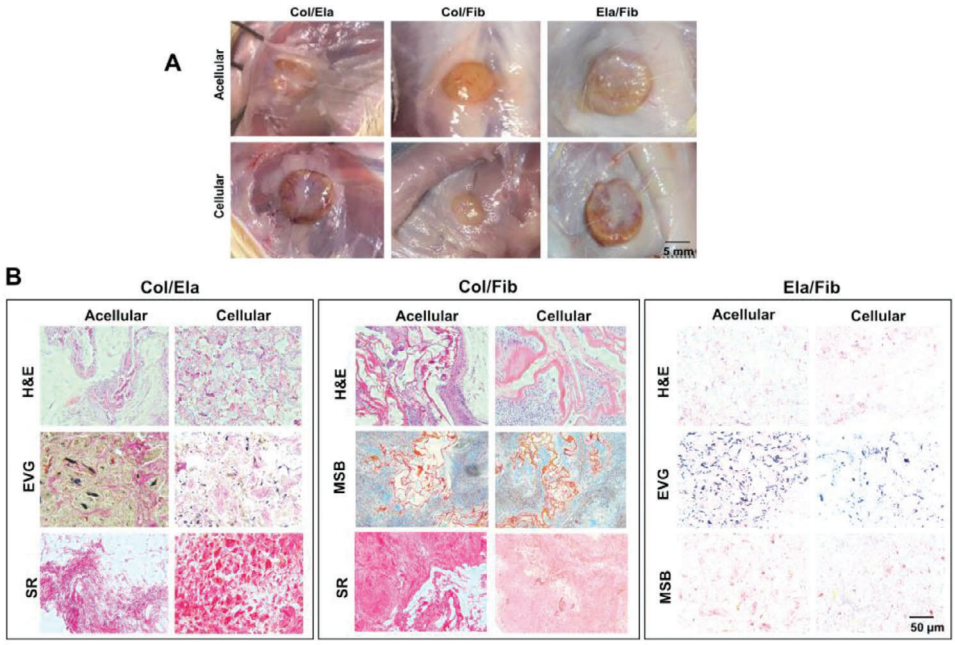

Figure 7. A) In vivo integration and gross observation. B) Differential stain for acellular and cellular scaffolds. Col/Ela: H&E, Sirius Red stain for collagen and Elastin Van Gieson (EVG) for elastin. Col/Fib: H&E, Sirius Red stain for collagen, and Martius Scarlet and Blue (MSB) for fibrin. Ela/Fib: H&E, EVG for elastin and MSB for fibrin.

of these scaffolds (Figure 6A). We found that Col/Ela had a vascular area of 8.24%. This may be attributed to the intrinsic characteristics of collagen and elastin, which are recognized for their ability to uphold vascular architecture and flexibility. In Col/Fib, results indicated a reduced vascular area of 2.43%. This implies that the combination of fibrin and collagen may not be as successful in boosting the growth of blood vessels on to the scaffold. The Ela/Fib scaffolds had a significant baseline vascular area of 19.66%, suggesting a robust capacity for angiogenesis. The synergistic effect of elastin and fibronectin seems to be highly efficacious, maybe because elastin offers structural reinforcement while fibronectin facilitates cellular connections that enhance the development of blood vessels. On the other hand, post inclusion of hADSCs (Figure 6B) resulted in a 12.54% increase in the vascular area in Col/Ela scaffolds and in Col/Fib seeded scaffold a substantial rise in vascular area of 12.69%. This indicates that hADSCs have the ability to greatly improve the angiogenic capacity of the Col/Ela and Col/Fib scaffolds. The combination of Ela/Fib had a significant level of vascularization, to 28.26% with the addition of hADSCs. The significant increase suggests that the Ela/Fib scaffold offers a highly favorable setting for hADSCs to express their angiogenic properties, by establishing an ideal scaffold for the integration and functioning of these cells.

These results indicated that hADSCs have the ability to greatly improve the formation of blood vessels in different scaffolds, with the degree of improvement variable depending on the composition of the scaffold. This suggests that the interplay between scaffold materials and biological components is essential for optimization. The findings emphasize the significance of selecting the appropriate blend of materials and cells to attain the intended outcomes for adipose tissue regeneration.

3.7. Adipogenesis

Gross observation (**Figure** 7A) showed that all scaffolds were able to integrate into the host tissue, and upon visual screening, there was no evidence of superficial inflammatory reaction. All the scaffolds showed angiogenic potential as we could see the invasion of blood vessels. These results could be correlated with the microscopy of H&E images (Figure 7B), which did not show the presence of inflammatory cell population. EVG and Sirius red staining showed that Col/Ela scaffolds' degradation was higher in the cellular group than in the acellular one. In contrast, for Col/Fib and Ela/Fib scaffolds, there was higher degradation in acellular than cellular. This was a result of tissue remodeling in the presence of ADSCs.[22] These factors played a vital role in adipogenesis, and we could quantify the presence of adipose tissue in our scaffolds (**Figure** 8A,B). Among these scaffold groups, Ela/Fib had the most adipogenic potential for both acellular and cellular groups than Col/Ela and Col/Fib scaffolds. This finding was evaluated further by immunohistochemistry. In this study, we used the same immunological markers as used in previous studies to understand the biological response to binary scaffolds: 1) DLK-1, an adipogenesis inhibitor, 2) PPARγ, an adipogenic transcriptional factor, 3) FABP4, adipogenesis at the cytoplasmic level and 4) Caveolin-1, an adipocyte cell membrane protein. DLK-1 is known as the molecular gatekeeper of adipogenesis which is cleaved by the tumour necrosis factor alpha (TNF-α) converting enzyme (TACE).[8,23] In our binary combination, the DLK-1 was not expressed in Col/Fib (cellular), and there was a marginal expression in all other scaffolds. This shows seeded ADSCs lost their stemness, and our scaffold did not arrest adipogenesis.[9] There is a well-established regime that PPARγ

© 2024 The Author(s). Macromolecular Bioscience published by Wiley-VCH GmbH

16165195, 0, Downloaded from https://onlinelibrary.wiley.com/doi/10.1002/mabi.202400073 by Universidad De Zaragoza, Wiley Online Library on [19/06/2024]. See the Terms and Conditions (https://onlinelibrary.wiley.com/terms-and-conditions) on Wiley Online Library for rules of use; OA articles are governed by the applicable Creative Commons License

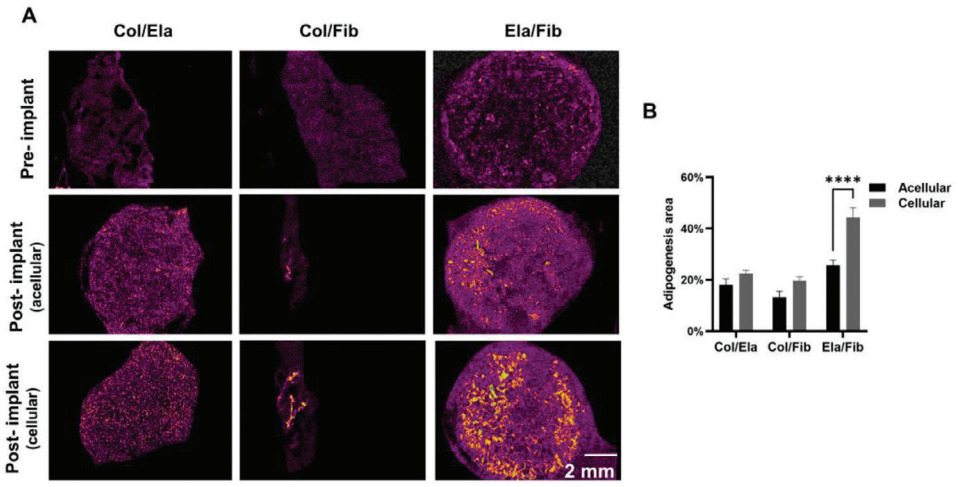

Figure 8. A) Adipogenesis analysis of 3D implanted scaffolds after 28 in vivo, and B) quantification of adipogenesis.

is a candidate adipogenesis regulator and promotes fat cell differentiation in vitro and in vivo.[10,11,24] Therefore, we evaluated the expression of PPARγ in our scaffolds. Col/Ela and Ela/Fib acellular groups had higher expression of PPARγ than cellular ones, whereas expression of PPARγ in Col/Fib acellular group was significantly lower than in cellularized scaffolds. In contrast, the expression of FABP4 in cellular Col/Ela and Ela/Fib was significantly higher than the acellular scaffolds. This could be due to Col/Fib scaffolds delayed adipogenesis of seeded hADSCs as PPARγ is a transcriptional factor and FABP4 is a cytoplasmic fatty acid chaperone of adipogenesis (**Figure 9**).[12,25] Adipocytes' cell membrane has caveolae, and caveolin-1 is abundantly expressed in mature cells; hence, we had analyzed our scaffolds for the caveolin-1 and found that Ela/Fib had significant higher expression in both acellular and cellular scaffolds than Col/Ela and Col/Fib scaffolds.

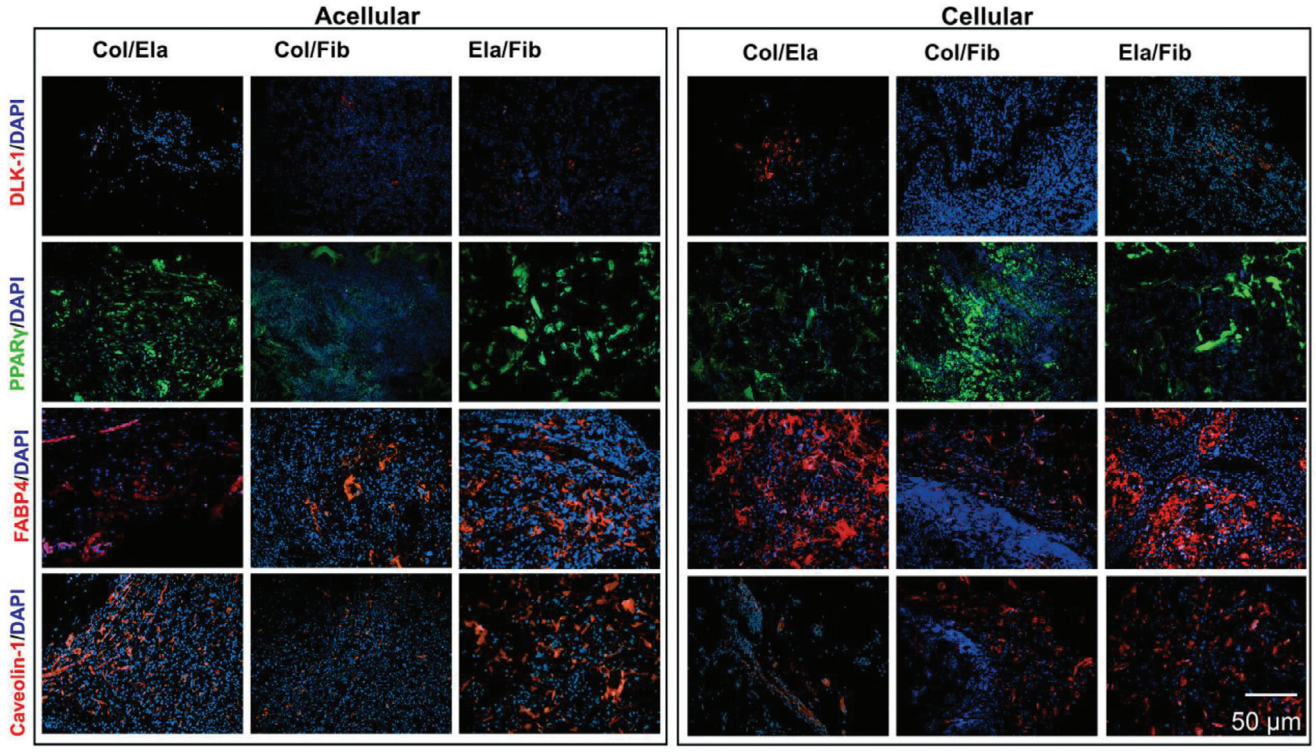

Figure 9. Immunofluorescence staining for Col/Ela, Col/Fib, and Ela/Fib in acellular and cellular groups. using DLK-1, PPARγ, FABP4 and Caveolin-1 antibodies.

© 2024 The Author(s). Macromolecular Bioscience published by Wiley-VCH GmbH

16165195, 0, Downloaded from https://onlinelibrary.wiley.com/doi/10.1002/mabi.202400073 by Universidad De Zaragoza, Wiley Online Library on [19/06/2024]. See the Terms and Conditions (https://onlinelibrary.wiley.com/terms-and-conditions) on Wiley Online Library for rules of use; OA articles are governed by the applicable Creative Commons License

4. Conclusion

This study undertook a comprehensive investigation into the physical and biological properties of scaffolds composed of Col/Ela, Col/Fib, and Ela/Fib. The 3D architectural properties of scaffolds were influenced by physical characteristics, such as the swelling ratio and water contact angle. Furthermore, the FTIR and thermal degradation characteristics of the binary compositions Col/Ela, Col/Ela-X, Ela/Fib, and Ela/Fib-X scaffolds demonstrate that the chemical structure and thermal stability of the binary scaffolds remain unaffected by glutaraldehyde crosslinking. Nevertheless, both Col/Fib and Col/Fib-X demonstrated thermal characteristics and secondary conformations of the proteins. The various scaffolds, when seeded with hADSCs, exhibit distinct differentiation potentials in the absence of external stimuli. While fibrin alone does not induce differentiation in hADSC, the combination of fibrin with collagen or elastin has been shown to enhance the scaffold's ability to promote differentiation. The results of the in vivo study indicate that Ela/Fib scaffolds exhibit a greater capacity for adipogenesis compared to Col/Ela and Col/Fib scaffolds, as evidenced by their superior angiogenic potential, ability to regenerate fat tissue, and expression of adipogenic markers. The investigation of this protein binary complex and its impact on the interaction between cells and materials has significantly enhanced our comprehension of adipose tissue regeneration.

Supporting Information

Supporting Information is available from the Wiley Online Library or from the author.

Acknowledgements

This work was supported by the Restoration of Appearance and Function Trust (UK Registered Charity No 299811) and the National Research Foundation (NRF) of Republic of Korea (Global Research Development Centre Program (2018K1A4A3A01064257), Priority Research Centre Program (2019R1A6A1A11034536), Medical Research Centre Program (2021R1A5A2022318), Basic science program (2018R1D1A1B07048020)), provided by the Ministry of Education or Ministry of Science and Technology, Republic of Korea. E.G.-G. was funded by a Ramon & Cajal Fellowship (RYC2021-033490-I, funded by MCIN/AEI/10.13039/501100011033, and the EU"Next GenerationEU/PRTR").

Conflict of Interest

The authors declare no conflict of interest.

Data Availability Statement

The data that support the findings of this study are available from the corresponding author upon reasonable request.

Keywords

adipose tissue engineering, ADSCs, fat regeneration, stem cells

Received: February 19, 2024
Revised: May 12, 2024
Published online:

[1] L. D. Kunda, K. R. Stidham, M. M. Inserra, P. S. Roland, D. Franklin, J. B. J. Roberson, *Otol Neurotol.* **2006**, *27*, 1078.
[2] P. Sawadkar, P. Sibbons, T. Ahmed, L. Bozec, V. Mudera, *ACS Biomater. Sci. Eng.* **2019**, *5*, 5218.
[3] R. Khan, M. H. Khan, *J. Indian Soc. Periodontol.* **2013**, *17*, 539.
[4] M. Meyer, *Biomed. Eng. Online* **2019**, *18*, 24.
[5] A. C. Brown, T. H. Barker, *Acta Biomater.* **2014**, *10*, 1502.
[6] C. H. Park, K. M. Woo, *Adv. Exp. Med. Biol.* **2018**, *1064*, 253.
[7] J. Ozsvar, C. Yang, S. A. Cain, C. Baldock, A. Tarakanova, A. S. Weiss, *Front. Bioeng. Biotechnol.* **2021**, *9*, 643110.
[8] W. F. Daamen, J. Veerkamp, J. Van Hest, T. Van Kuppevelt, *Biomaterials* **2007**, *28*, 4378.
[9] S. M. Mithieux, A. S. Weiss, *Adv. Protein Chem.* **2005**, *70*, 437.
[10] S. D. Shapiro, S. K. Endicott, M. A. Province, J. A. Pierce, E. J. Campbell, *J. Clin. Invest.* **1991**, *87*, 1828.
[11] Y.-b. Chen, C.-h. Chen, Z. Qixu, Y. Han, *J. Tissue Eng.* **2016**, *20*, 1508.
[12] J. Zhang, Y. Liu, Y. Chen, L. Yuan, H. Liu, J. Wang, Q. Liu, Y. Zhang, *Stem Cells Int.* **2020**, *2020*, 8810813.
[13] P. Sawadkar, N. Mandakhbayar, K. D. Patel, J. O. Buitrago, T. H. Kim, P. Rajasekar, F. Lali, C. Kyriakidis, B. Rahmani, J. Mohanakrishnan, *J. Tissue Eng.* **2021**, *12*, 20417314211019238.
[14] P. Sawadkar, N. Mandakhbayar, K. D. Patel, J. O. Buitrago, T. H. Kim, P. Rajasekar, F. Lali, C. Kyriakidis, B. Rahmani, J. Mohanakrishnan, R. Dua, K. Greco, J. H. Lee, H. W. Kim, J. Knowles, E. Garcia-Gareta, *J. Tissue Eng.* **2021**, *12*, 20417314211019238.
[15] N. P. Podolnikova, S. Yakovlev, V. P. Yakubenko, X. Wang, O. V. Gorkun, T. P. Ugarova, *J. Biol. Chem.* **2014**, *289*, 2371.
[16] P. Sawadkar, J. Mohanakrishnan, P. Rajasekar, B. Rahmani, N. Kohli, L. Bozec, E. Garcia-Gareta, *ACS Appl. Mater. Interfaces* **2020**, *12*, 13587.
[17] S. J. Huang, R. H. Fu, W. C. Shyu, S. P. Liu, G. P. Jong, Y. W. Chiu, H. S. Wu, Y. A. Tsou, C. W. Cheng, S. Z. Lin, *Cell Transplant* **2013**, *22*, 701.
[18] M. T. Gonzalez-Garza, D. E. Cruz-Vega, A. Cardenas-Lopez, R. M. de la Rosa, J. E. Moreno-Cuevas, *Am. J. Stem Cells* **2018**, *7*, 38.
[19] P. Sawadkar, N. Mandakhbayar, K. D. Patel, J. O. Buitrago, T. H. Kim, P. Rajasekar, F. Lali, C. Kyriakidis, B. Rahmani, J. Mohanakrishnan, R. Dua, K. Greco, J.-H. Lee, H.-W. Kim, J. Knowles, E. García-Gareta, *J. Tissue Eng.* **2021**, *12*, 20417314211019238.
[20] Y. Cao, *Nat. Rev. Drug Discovery* **2010**, *9*, 107.
[21] S. Saberianpour, M. Heidarzadeh, M. H. Geranmayeh, H. Hosseinkhani, R. Rahbarghazi, M. Nouri, *J. Biol. Eng.* **2018**, *12*, 36.
[22] L. Ghasemi-Mobarakeh, M. P. Prabhakaran, L. Tian, E. Shamirzaei-Jeshvaghani, L. Dehghani, S. Ramakrishna, *World J. Stem Cells* **2015**, *7*, 728.
[23] Y. Wang, H. S. Sul, *Mol. Cell. Biol.* **2006**, *26*, 5421.
[24] H. S. Park, U. I. Ju, J. W. Park, J. Y. Song, D. H. Shin, K. H. Lee, L. S. Jeong, J. Yu, H. W. Lee, J. Y. Cho, S. Y. Kim, S. W. Kim, J. B. Kim, K. S. Park, Y. S. Chun, *Cell Death Differ.* **2016**, *23*, 1296.
[25] M. Furuhashi, S. Saitoh, K. Shimamoto, T. Miura, *Cardiology* **2014**, *8*, 23.

© 2024 The Author(s). Macromolecular Bioscience published by Wiley-VCH GmbH

16165195, 0, Downloaded from https://onlinelibrary.wiley.com/doi/10.1002/mabi.202400073 by Universidad De Zaragoza, Wiley Online Library on [19/06/2024]. See the Terms and Conditions (https://onlinelibrary.wiley.com/terms-and-conditions) on Wiley Online Library for rules of use; OA articles are governed by the applicable Creative Commons License